Analyst

Accepted Manuscript



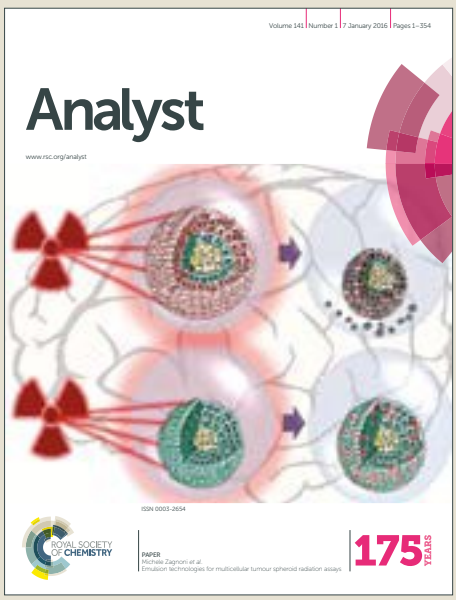




ROYAL SOCIETY OF CHEMISTRY

rsc.li/analyst

View Article Online
DOI: 10.1039/C8AN01127C

Journal Name

ARTICLE

# Multiplex detection of urinary miRNA biomarker by transmission surface plasmon resonance

Received 00th January 20xx,
Accepted 00th January 20xx

DOI: 10.1039/x0xx00000x

www.rsc.org/

Wing Kiu Yeung[a] , Huai-Yi Chen,[a,b,c] , Juan-Jie Sun[a], Tung-Han Hsieh[a], Mansoureh Z. Mousavi[d], Hsi-Hsien Chen[g,h], Kuang-Li Lee[a,e], Heng Lin[f], Pei-Kuen Wei[a] and Ji-Yen Cheng [a,i,j,k]

Clinical assessment of short-stranded nucleic acid biomarkers such as miRNAs could potentially provide useful information for monitoring disease progression, prompting definitive treatment decisions. In the past decade, advancement in biosensing technology have shifted towards rapid, real-time and label-free detection systems, in such surface plasmon resonance (SPR) biosensors-based technology has been of high interest. Here, we developed an automated multiplex transmissive surface plasmon resonance (t-SPR) platform with the use of capped gold nanoslit integrated microfluidic surface plasmon resonance (SPR) biosensor. The automated platform was custom designed to allow analysis of the spectral measurement using the wavelength shift (dλ), intensity (dI) and the novel area change (dA) for surface binding reactions. A simple and compact nanostructure based biosensor was fabricated with multiplexed real-time detection capability. The sensitivity and specificity of the microfluidic device was demonstrated through the use of functionalised AuNP for target molecule isolation and signal enhancement in combination with probes on the CG nanoslit surface. Our work allows multiplex detection of miRNA at femtomolar concentration in complex medium such as urine.

## 1. Introduction

A decade of research on short-stranded nucleic acids such as DNA and miRNA has provided us useful information on basis of disease for diagnosis and have aided the development for powerful tools for assessing treatment efficacy (1). These short-stranded nucleic acids play a vital role in controlling human gene expressions and are important in virtually all biological functions(2). Dysregulation of the nucleic acid expression level has been correlated with human infection disease by virus, bacteria (3), as well as cancer(4, 5) ,nervous system disorder (7), bone disease (6, 7) and diabetes(8, 9). Disease progression can be expressed by the nucleic acids level (10), this characteristic can be translated into a platform for multiphasic disease diagnostics. The conventional approach to examine the level of miRNA or DNA in blood or other bodily fluids are commonly conducted with molecular diagnostic tools such as polymerase chain reaction (PCR) based (3) or enzyme-linked immunosorbent assay based (ELISA) (10). These methods take advantages of the highly specific hybridisation process of the capturing probe to the target molecules. Despite demonstrated to be highly sensitive with a detection limit in the femtomolar range (12), these methods are highly complex, time-consuming, expensive and require experienced operators. Advances in new branches of studies involving the miRNA microarray and *in situ* hybridization methods have become mature and began its use in clinical practice. Majority of these methods use targets that have been chemically and/or enzymatically modified with fluor-labelled 3' capturing probe and a second 5' probe for specific sequence detection (11-13). The design of complementary probes used have demonstrated high sensitivity and specificity but the major drawback of fluor-labelling with the highly modified target is the long sample preparation time and experimental cost.

The detection of miRNA can also be done using optical techniques such as surface plasmon resonance (SPR), a surface-based detection. SPR is an optical detection method that allows monitoring of the real-time kinetic behaviour between the target molecules and the capturing probe by examining the change in the refractive index (RI) at the sensor surface. SPR detection systems have been widely studied and the integration with microfluidic technology has shown very promising results for biosensing applications (14-17). Conventional SPR devices employ the Kretschmann configuration, which requires a complex and costly prism-coupling set-up for precise theta-

[a] Research Center for Applied Science, Academia Sinica, Taiwan
[b] Department of Engineering and System Science, National Tsing Hua University, Taiwan
[c] Nano Science and Technology Program, Taiwan International Graduate Program, Academia Sinica and National Tsing Hua University, Taiwan
[d] Istituto Italiano Di Tecnologia, Genova, Italy
[e] Institute of Physics, Academia Sinica, Taiwan
[f] Department of Physiology, School of Medicine, College of Medicine, Taipei Medical University, Taipei, Taiwan
[g] Division of Nephrology, Department of Internal Medicine, School of Medicine, College of Medicine, Taipei Medical University, Taipei, Taiwan
[h] Division of Nephrology, Department of Internal Medicine, Taipei Medical University Hospital, Taipei, Taiwan
[i] Department of Mechanical and Mechantronic Engineering, National Taiwan Ocean University
[j] Institute of Biophotonics, National Yang-Ming University, Taipei, Taiwan
[k] College of Engineering, Chang Gung Engineering, Taoyuan, Taiwan
† Footnotes relating to the title and/or authors should appear here.
Electronic Supplementary Information (ESI) available: [details of any supplementary information available should be included here]. See DOI: 10.1039/x0xx00000x

View Article Online
DOI: 10.1039/C8AN01127G



theta measurements (18, 19). Meanwhile, metallic periodic nanostructure-based (namely nanoslits and nanoholes) SPR sensors exploit the extraordinary optical transmission (EOT) phenomenon, resulting in an asymmetric Fano resonance in the transverse magnetic (TM) polarised transmitted spectra (20). This interesting feature allows miniaturization of SPR sensors and enlargement of the sensing area. Regardless of the SPR method used, the detection of binding relies on the change in the refractive index at the sensor surface. Molecules such as miRNA are comparatively small (19 – 23 mer) and the change in RI is very restricted, resulting in a low SPR signal change and thus high detection limit. In order to amplify the signals, many attempts such as employing nano-composites (20, 21), antibodies and proteins (22) and magnetic beads (23) have been conducted. These methods take advantage of the bio/metallic particles' ability to hybridize or perform cleavage reactions with the target and proceed into a sandwich assembly on the SPR sensing surface. This results in a strong plasmon-exciton coupling and hence a large increase of the SPR signal.

As an extension of the previous work from our group (23, 24) a multiplex miRNA automated detection platform is presented in this work. A highly sensitive capped gold (CG) nanoslit was used as the sensor to detect low concentration of target molecules in urine. Compared to the previous work, the use of gold nanoparticles (AuNP) instead of magnetic particles (MNP) is used as a signal enhancer. The advantages of using AuNP over MNP is the ability to remove any additional equipment such as magnets to provide an external force and allows the development into a simpler controllable automated device. More importantly, this platform is a multiplexing SPR biosensor with built-in a novel spectral analysis approach to reduce the detection limit of the Fano peak change with the progression of target molecule binding. Multiplex analysis of miRNA is highly desired for clinical settings, as it allows an increase in the predictive power for a particular disease.

## 2. Materials and Method

### 2.1. Double hybridisation sensing method

The double hybridisation method is designed to allow highly specific detection of target miRNA molecules and reduce the non-specific binding in a complex sample such as urine. In this work, AuNPs and CG nanoslits were functionalised with bead probe and monitoring probe, respectively. In brief, the functionalised AuNP was introduced to the sample to capture and tag the target molecule. The AuNP carrying the target molecules were introduced to the monitoring probe on the CG nanoslit surface. The hybridization of the target molecules to the monitoring probes leads to a change in the RI on the CG nanoslit surface, allowing direct measurement of the kinetic binding. The schematic illustration of the experiment is shown in **Fig. S1.**

#### 2.1.1. Functionalisation of the CG nanoslit surface

The capped gold nanostructure was fabricated using methods previously mentioned (18, 25), using a homemade hot embossing nanoimprinting machine. After imprinting the nanostructures on the plastic film, the CG nanoslit surface was cleaned with oxygen plasma to remove any residuals on the surface prior to gold sputtering (**Fig.1a**). The cross-sectional schematic diagram of the periodic nanostructures as shown in Fig. 1a have an area of 5 mm X 5 mm and a ridge height of 45 ± 2 nm (**Fig. 1b**). The Finite Difference Time Domain (FDTD) was applied to simulate the Fano peak as used by Ng *et al* (26). The results are shown in Supplement 3

The CG nanoslit surface was immobilised with monitoring probe (100 µM, 1 X Tris-EDTA buffer), which is a 22-mer nucleotide with an 11-mer spacer (T) and 11-mer sequence complementary to the 5' half of the target sequence. The 3' terminal of the monitoring probe is attached to the CG nanoslit surface through thiol bonding. The four monitoring probes (I, II, III and R) were designed in this work.

The 4 monitoring probe solutions were pipetted manually onto the 4 regions of the CG nanoslit surface forming 4 independent sensing areas, as displayed in **Fig.2**. To prevent liquid evaporation and contamination, the immobilization process was conducted in an air-tight petri dish with temperature and humidity controlled at 22 ± 5 °C and 39 ± 5%, respectively for 12 hours. The CG nanoslit was then washed in ddH2O twice to remove excess probe on the surface. The successfulness of the immobilisation process was confirmed by the formation of 4 isolated hydrophilic regions on the CG nanoslit surface. Further confirmation of the successful immobilization was provided by the Fano peak changes, as described below.

#### 2.1.2. Functionalisation of the AuNPs

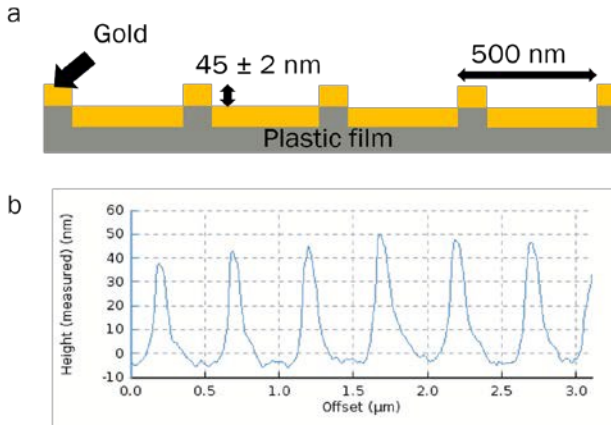


Fig.1 (a) The schematic configuration depicts the geometric of the capped gold (CG) nanoslit structure. (b) The cross-sectional profie measurement across the CG nanooslit surface.- match the gold thickness to ridge height for hgiher sensitivity.

Gold nanoparticles (AuNPs) act as the signal amplifier in our work. In order to functionalise the AuNPs, 1 ml from the stock solution (4.94 x $10^{12}$ particles / mL) of the commercially available nanoparticles (Nanocomposix, CA, d= 10 nm) were centrifuged at 16,000 x g for 1 hour and re-suspend with 0.5 ml of 0.1 X PBS. Subsequently, 25 µl of the bead probe solution

View Article Online
DOI: 10.1039/C8AN01276



(100 uM, 1 X Tris-EDTA buffer) was added to the AuNP suspension. The bead probe is a 22-mer 5' thiol-modified probe with an 11-mer spacer (T) and 11-mer moiety complementary to the 3' half of the target sequence. The suspension was left overnight on a rocker and was then centrifuged for 15 min, and re-suspend with 1 ml of 0.1 X PBS to remove any unbounded probes. Four bead probes (I, II, III and R) were designed and used to functionalised the AuNP using the method described, forming I-NP, II-NP, III-NP and R-NP, respectively.

### 2.2. Fabrication of the integrated microfluidic chip

The microfluidic device used in this work is designed for detecting short-stranded nucleic acids using transmission surface plasmon resonance (t-SPR) detection technique and is displayed in Fig. 2. The disposable microfluidic device is a multilayer structure fabricated using a $CO_2$ laser scriber on polymethylmethacrylate (PMMA) sheet and double-sided tape (3M™ clear adhesive SR7625) with an integrated CG nanoslit as the biosensor. The microfluidic chip was designed to protect and provide a rigid structure to allow the CG nanoslit sensor surface to be maintained in perpendicular to the incident light. It must be born in mind that the Fano resonance is a result of the two-mode coupling between the cavity resonance and the SPR modes on the nanoslit structure, thus it is highly sensitive

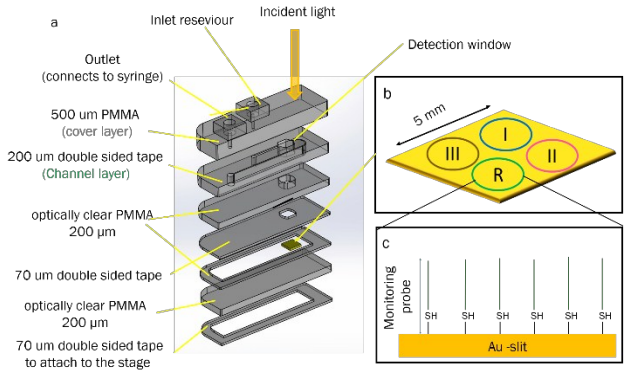


Fig. 2 (a) The schematic diagram illustrating the layers within the integrated microfluidic t-SPR chip. (b) The four independent sensing arragement on the CG nanoslit surface with one marked as reference. (c) Scehmatic illustratio of the immobolised biosensor with monitoring probe

to the incoming light angle. And therefore, maintaining the sensor surface in perpendicular to the normal incident light can ensure the transmission spectra recorded are formed under the same coupling method.

The cover layer of the microfluidic chip displayed in Fig. 2 could effectively reduce sample evaporation and contamination during the experiment. The adaptors attached to the inlet acts as a reservoir that holds up to 250 µl of the sample fluid. The outlet adaptor is connected through a tubing to a syringe (please see below).

### 2.3. Platform assembly and working principle

All the transmission SPR measurements were performed using a custom-built t-SPR automated platform as shown in Fig. 3. A C-shape frame made of Al-alloy was designed to hold the optical components and maintain a rigid and firm optical path. The stabilised light source (SLS 201 L, Thorlab, USA) was coupled with a 230 µm optical fibre and the collimator 1 (F220SMA-780, Thorlab, USA). The collimated light then passes through a 1.5 mm pinhole before transmitting through the sensing area (CG nanoslit) in the microfluidic chip. The integrated microfluidic chip is placed into the chip holder that is attached to the computer programmable XY stage. The XY stage was set at a speed of 28 mm/min, and the stage is programmed to hold at designated position prior to spectral measurement. The advantage of stopping the stage prior to spectral measurement includes 1) correct sample positioning and alignment with respect to the optical system, 2) minimise mechanical induced fluctuations to the spectral measurement.

Meanwhile, the outlet adaptor of the integrated microfluidic chip is connected to a syringe and a syringe pump (NE-1000, New Era Pumping system) and it is operated in withdrawal mode to provide the desired flow rates through the detection window, and the syringe is used to collect the waste. The use of withdrawal pumping effectively prevent unwanted bubbles.

View Article Online
DOI: 10.1039/C8AN01127C

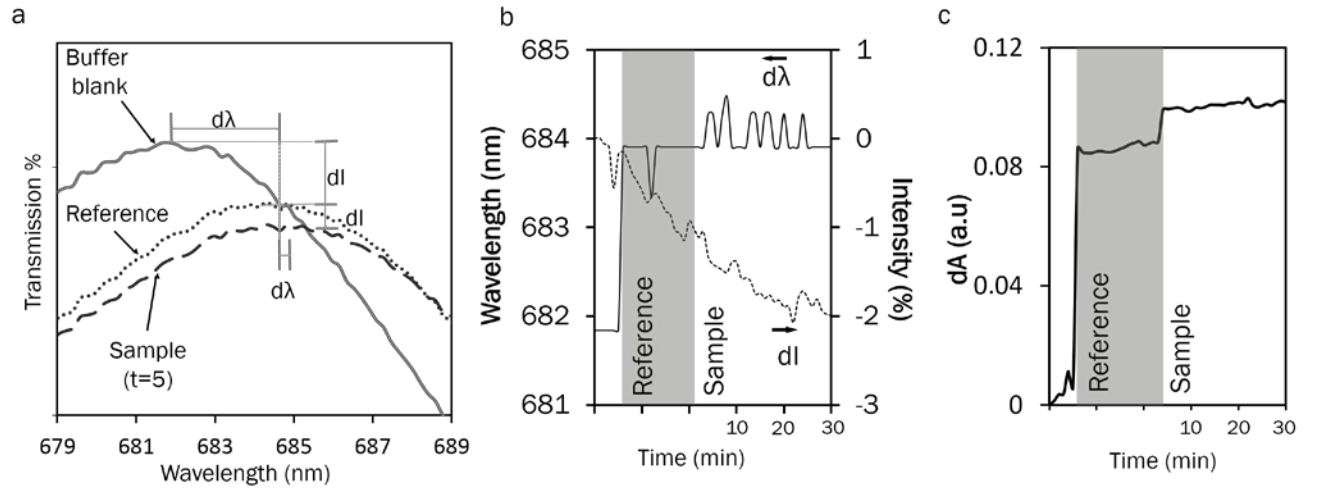


Fig. 4 (a) A represntation of the transmission % spectra obtained at various stages of the singleplex experiment (Buffer blank, Reference and 5 mins after sample injection) It marks the changes in wavelength and intensity between the stages; (b) The dynamic response of the Fano peak analysed in terms of wavelength change (dλ), intensity change (dI); and (c) area change (dA).

The incident light transmitted through the sensor surface, and passed the polarizer to remove the transverse electric (TE) polarized light. Thereby, the transverse magnetic (TM) light is collected through collimator 2, and passing through a 230 µm optical fibre that is connected to a spectrometer (Model: USB 4000, Ocean Optics). The optical path of the platform is shown in **Fig. S2**. The spectrum measurement parameter is controlled by a custom designed LabVIEW program (National instrument, USA) provided by the manufacturer, and each spectrum recorded consisted of an average of 100 individual spectra (integration time 6000 ms) and was further processed into transmission spectra using Eq. 1.

$$T(\%) = \frac{(S_\lambda - D_\lambda)}{(R_\lambda - D_\lambda)} \times 100\% \qquad \text{(Eq. 1)}$$

Where $S_\lambda$, $D_\lambda$ and $R_\lambda$ are the sample spectrum, dark spectrum and light source reference spectrum, respectively. The custom designed LabVIEW software is packaged into an execution application which allows distribution. The software consists of data acquisition, analysis and report generation, which is desired for POC applications as it can quickly provide information results on site of the measurement **(Fig. S3).** In order to analyse the Fano peak spectral changes over time, the software identifies the Fano peak at the initial stage of the experiment by determining the maximum point within a fixed wavelength range (680 ± 10 nm), marking the initial Fano peak wavelength ($\lambda_{0,\,max}$). The area under that Fano peak is calculated as the sum of the intensity within a fixed wavelength range ($\lambda_{0,\,max}$± 10 nm). The measurements were programmed to record one measurement per minute for each sensing region. Thus, the peak area changes over time was calculated with respect to the changes in intensity at each wavelength within the Fano peak range, compared to that of t = 0, it can be expressed as Eq. 2

$$dA = \sum_{\lambda} |(I_\lambda(t) - I_\lambda(0)| \qquad \text{(Eq. 2)}$$

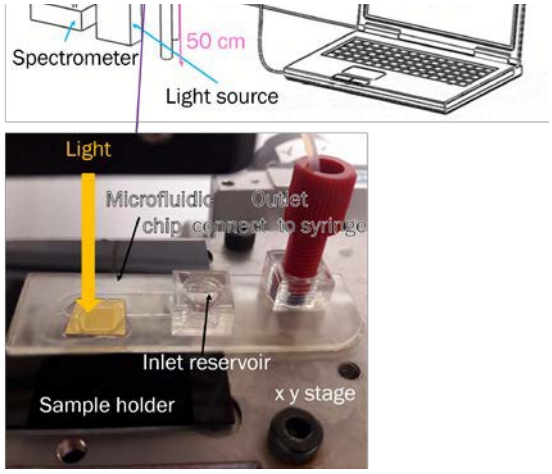


Fig. 3 Schematic representation of the custom-designed t-SPR automated platform set-up. A stabilized light shines collimated light onto the sensor surface and captured by the miniaturized spectrometer. The X Y stage and the spectrometers are controlled by the in-build LabVIEW software. The immobilized CG nanoslit integrated microfluidic chips were mounted onto the sample holder on the programmable X Y stage.

Where $I_\lambda(t)$ and $I_\lambda(0)$ are the intensity of the spectra at each wavelength in the Fano peak range.

### 2.4. Binding homogeneity measurements

The uniformity of the SPR sensing regions is utmost important to ensure results are not biased, the homogeneity was assessed as follows. Monitoring probe III was immobilised onto the CG nanoslit surface in the integrated microfluidic chip using manual drop method. The measurement was carried out in three stages; buffer, reference and sample stage. During the buffer stage, the buffer solution (0.1 X PBS) was introduced to the CG

View Article Online
DOI: 10.1039/C8AN01276



nanoslit surface using a withdrawal rate of 150 µl/min for 1 min, then the withdrawal rate was reduced to 10 µl/min for 4 minutes. The initial high withdrawal rate was designed to eliminate bubbles that may developed within the channels, and furthermore it can be used to examine the quality of the chip and ensure no leaking of the microfluidic chip channels. This results from this buffer stage also acts as the baseline measurement.

To measure the specificity of the sensor surface, a reference solution (250 µl) containing I-NP, II-NP, III-NP, R-NP and R-target mixed in buffer solution was loaded into the inlet reservoir. The final concentration of the R-target in the reference solution was fixed at 330 fM. Using a syringe pump, the solution was withdrawn from the outlet and through the CG nanoslit surface. The withdrawal flow rate was 150 µl/min for 1 min, then reduced to 10 µl/min for 9 min. The total time for the reference stage was 10 min. Immediately before the reference solution drains out in the reservoir, 240 µl of the sample solution was loaded into the inlet reservoir. The sample solution contains all four functionalised AuNP (I-NP, II-NP, III-NP and R-NP) and their complementary target molecules. In such, the R-target concentration was set as 330 fM as it was in the reference stage, meanwhile, III-target was added to the sample solution with the final concentration at 167 fM. The withdrawal flow rate was set at 150 µl/min for 1 min, then the withdrawal rate was reduced to 10 µl/min for 29 min, making the total sample stage to be 30 min. All responses were reported as the mean average dA values derived from measurements between those at initial buffer (PBS) stage and end sample stage (30 min after sample injection) ± standard deviation.

### 2.5. Multiplex kinetic measurements

To investigate the multi-target miRNA detection potential of this platform. The CG nanoslit that was immobilised with 4 different monitoring probes (I, II, III and R) as mentioned previously, and was integrated in the microfluidic chip. In this section, synthetic targets were spiked into healthy volunteers' urine samples instead of PBS buffer. This research project was approved by the Institutional Review Board of the Department of Internal Medicine, Taipei Medical University Hospital, and informed consents were obtained from all volunteers. These samples were obtained from 6 healthy volunteers, and were frozen at -80 °C until use. The urine sample was centrifuged at 16,000 x g for 10 min to remove debris before mixing with the target spiked urine samples. Same withdrawal steps as those used in Section 2.4.

### 2.6. Statistical analysis

Statistical analysis of data was performed using two-way ANOVA to test differences between samples. Differences were considered as significant when the *p*-value was less than 0.05.

## 3. Results and Discussion

### 3.1. Uniformity and functionality of the microfluidic chip

**Fig. 4a** shows the transmissive Fano spectra under different media for a normal-incident TM polarised light obtained from the homogeneous binding singleplex experiment. For CG nanoslit structures with a period of 500 nm, the measured Fano resonance at the water/gold interface was 665 ± 1 nm (18). From our software, the initial Fano peak ($\lambda_0$ max) in our measurement is determined and found to be at 681.8 nm. The redshift of the Fano peak from the water/gold interface indicates successful immobilisation of the monitoring probe on the CG nanoslit surface. The calculated transmission spectra and resonance field distribution of the CG nanoslit used in this experiment using finite difference time domain (FDTA) method is shown in Fig. S4

The introduction of the reference solution leads to a drastic red-shift and reduction in the peak intensity. This can be explained by the dramatic change in the bulk buffer reflective index (RI) from PBS buffer to AuNP containing solution. The Fano peak position (λ max) change over time throughout the three stages is displayed in Fig. 4b. As the sample solution was introduced to the microfluidic chip, a 2.2 ± 0.2 nm red-shift was observed. The signal fluctuation was comparatively high and reaching the optical resolution of the spectrometer.

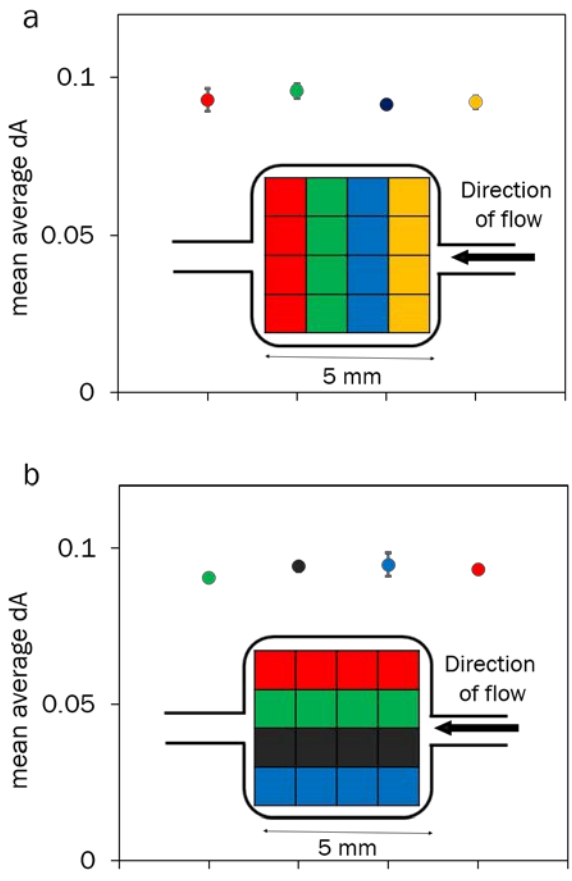


Fig. 5 The plot representing the change in Fano peak area in respect to the capturing sensitivity of immobilised CG nanoslit through the (a) longitudinal and (b) horizontal direction passing from the inlet to the outlet port in the detection window. The error bar represents the standard error of the mean.

View Article Online
DOI: 10.1039/C8AN01257C



Meanwhile, the Fano peak intensity continuous to decrease throughout the three stages of the experiment. It can be observed that using the two conventional analysis methods, it is difficult to distinguish the data obtained from the reference to those from the sample stage. Thereby, these analysis methods may not be suitable for detecting low concentration of short-stranded molecules.

The change in Fano peak area over time (dA) is displayed in **Fig. 4c.** A prominent change in the dA value is observed at each stage of the experiment, in particular, the change in dA value from the reference and sample stage marks the immediate influence of complementary target molecules to the RI on the sensor surface. These results indicate the dA analysis method is comparatively more suitable for detecting low concentration target molecules. This is in good agreement with the RIR calculations using different analysing algorithms (Fig. S5)

The standard deviation of the SPR response fluctuation from surface to be statistically insignificant from each other. This can be deduced that there are insignificant differences between the upper and lower stream of the sensor surface with respect to the flow direction.

### 3.2. Multiplex detection of synthetic target spiked in urine

The ability for detecting multiple biomarkers in one microfluidic chip is highly desired for disease diagnosis, as it can rapidly provide a disease profile of the patient's severity. To evaluate the specificity, sensitivity and the multiplex ability of our platform, the CG nanoslit was immobilised with 4 different monitoring probes (I, II, III and R) as mentioned in **Fig. 2.** The reference spot was used as an internal positive control and to examine the selectivity of our biosensor.

**Fig. 6a** illustrated the relation between the change in Fano peak area (dA) and the concentration of the target molecules

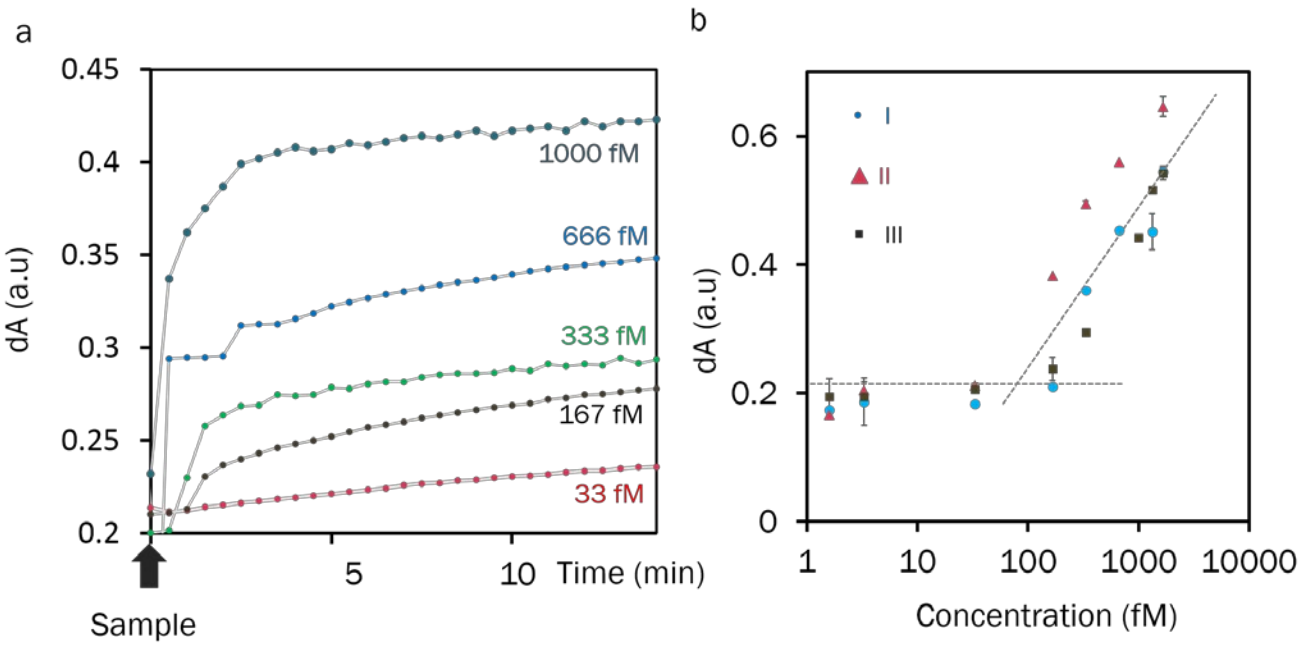


Fig. 6 (a) Real-time monitoring of the kinetic binding between the functionalised AuNP carrying the target sequence and the monitoring probe on the CG nanoslit surface. (b) The calibration curve obtained for various concentration of the target I, II and III spiked in urine from healthy participants. The dA value is obtained from those at steady state (20 min after sample injection). The equations obtained from the linear regresision of the calibration curve is y = 0.1422ln(x) – 0.4913 ($R^2$ = 0.9657), y=0.1115ln(x) – 0.1717 ($R^2$ =0.9797) and y = 0.1356ln(x) – 0.4732($R^2$=0.9802) for synthetic target I, II and III, respectively. The error bar represents the standard error of the mean.

in the sample stage at t = 25 – 30 was 0.00048, which is considered as the background noise of this part of the experiment. Thus, using the dA calculation can significantly improve the signal-to-noise ratio (S/N) of our t-SPR platform.

The data from the homogeneity measurements were therefore analysed using the dA method to examine the binding uniformity of target molecules to the monitoring probes. Examination of the longitudinal and horizontal regions across the CG nanoslit passing through the CG nanoslit chamber is displayed in **Fig. 5a and b**, respectively. It indicated the mean average dA values obtained from different regions of the sensor using our platform. A measurable increase in the dA response is observed with the target concentration from 166 fM or higher. Compared to previous work by Nie *et al* (21) using AuNPs amplified SPR method on miRNA targets, which resulted the minimum target concentration detected to be 1 pM. This work has demonstrated significant improvement on the detection limit.

In addition, it must be born in mind that for most surface-based sensors, the signals are relying on the accumulation of the target molecules which is determined by the analyte mass transport (27). In aim to enhance the performance, previous



 

work by Mousavi *et al* (23) and Nie *et al* (21) have proposed increasing hybridisation time between the functionalised particles and the target molecules and/or the target molecules with the monitoring probe on the Au film surface, up to 60 mins. Their work proposed the SPR signal increased with time, and plateau at 60 min. In relation to our work, the urine sample was not left to hybridise with the functionalised AuNP for 1 hour prior to measurements. More importantly, despite the sample was flown through the sensor for 30min, it can be observed at the signals have reached plateau within 15 min. Therefore, the whole experiment time including sample preparation can be drastically reduced. As all the dA signal reached a plateau at 15 min after sample injection, therefore the dA value at 20 min was selected to determine the relation between dA value and the concentration of targets in a multiplex detection set-up.

**Fig. 6b** illustrates the logarithmic relation between the dA value and the concentration of the short-stranded target molecules. Since a dA value larger than 0.2 was regarded as signal for the measurement, it was estimated that this current platform allows detection of miRNA in multiplex measurement set-up with the limit of detection around 30 fM. These results demonstrated the high sensitivity of the method to detect low concentration of the target molecule without labelling or complex sample treatment in a complex media. This work has shown to be very promising for multiplex biosensing applications for short-stranded nucleic acid at low concentration.

## 4. Conclusion

In this paper, we presented an automated multiplex t-SPR sensing platform using a novel signal processing method to enhance the sensitivity of the device. The dA calculation method has demonstrated to enhance the sensitivity of the platform while lowering the background noise. The multiplexing ability of our device was examined by detecting 3 biomarkers and a control spiked into healthy urine samples from healthy patients. The results showed a measurable t-SPR signal was obtained after only 10 min of sample injection at a femtomolar concentration of the target molecules. The small volume multiplex format that provides a rapid detection which is highly preferable for the development of t-SPR into point-of-care devices.

## Conflicts of interest

There are no conflicts to declare.

## Acknowledgements

The acknowledgements come at the end of an article after the conclusions and before the notes and references. Notes and references

1. Taton TA, Mirkin CA, Letsinger RL. Scanometric DNA array detection with nanoparticle probes. Science. 2000;289(5485):1757-60.
2. Bartel DP. MicroRNAs: Genomics, Biogenesis, Mechanism, and Function. Cell. 2004;116(2):281-97.
3. Verma P, Pandey RK, Prajapati P, Prajapati VK. Circulating MicroRNAs: Potential and Emerging Biomarkers for Diagnosis of Human Infectious Diseases. Frontiers in Microbiology. 2016;7(1274).
4. Reddy KB. MicroRNA (miRNA) in cancer. Cancer Cell International. 2015;15:38.
5. Iorio MV, Ferracin M, Liu CG, Veronese A, Spizzo R, Sabbioni S, et al. MicroRNA gene expression deregulation in human breast cancer. Cancer Res. 2005;65(16):7065-70.
6. Hackl M, Heilmeier U, Weilner S, Grillari J. Circulating microRNAs as novel biomarkers for bone diseases – Complex signatures for multifactorial diseases? Molecular and Cellular Endocrinology. 2016;432:83-95.
7. Kim KM, Lim S-K. Role of miRNAs in bone and their potential as therapeutic targets. Current Opinion in Pharmacology. 2014;16:133-41.
8. Simpson K, Wonnacott A, Fraser DJ, Bowen T. MicroRNAs in Diabetic Nephropathy: From Biomarkers to Therapy. Current Diabetes Reports. 2016;16:35.
9. Feng J, Xing W, Xie L. Regulatory Roles of MicroRNAs in Diabetes. International Journal of Molecular Sciences. 2016;17(10):1729.
10. Chan KK, Liu Z, Xie Z, Chiu M, Wang H, Chen P, et al. A Novel Ultrasensitive Hybridization-Based ELISA Method for 2-Methoxyphosphorothiolate MicroRNAs and Its In vitro and In vivo Application. The AAPS Journal. 2010;12(4):556-68.
11. Geiss GK, Bumgarner RE, Birditt B, Dahl T, Dowidar N, Dunaway DL, et al. Direct multiplexed measurement of gene expression with color-coded probe pairs. Nature Biotechnology. 2008;26:317.
12. Wark AW, Lee HJ, Corn RM. Multiplexed detection methods for profiling microRNA expression in biological samples. Angewandte Chemie International Edition. 2008;47(4):644-52.
13. Wark AW, Lee HJ, Qavi AJ, Corn RM. Nanoparticle-Enhanced Diffraction Gratings for Ultrasensitive Surface Plasmon Biosensing. Analytical Chemistry. 2007;79(17):6697-701.
14. Malic L, Morton K, Clime L, Veres T. All-thermoplastic nanoplasmonic microfluidic device for transmission SPR biosensing. Lab on a Chip. 2013;13(5):798-810.
15. Nahavandi S, Baratchi S, Soffe R, Tang S-Y, Nahavandi S, Mitchell A, et al. Microfluidic platforms for biomarker analysis. Lab on a Chip. 2014;14(9):1496-514.
16. Tokel O, Inci F, Demirci U. Advances in Plasmonic Technologies for Point of Care Applications. Chemical Reviews. 2014;114(11):5728-52.
17. Tokel O, Yildiz UH, Inci F, Durmus NG, Ekiz OO, Turker B, et al. Portable Microfluidic Integrated Plasmonic Platform for Pathogen Detection. Scientific Reports. 2015;5:9152.
18. Lee KL, Wu TY, Hsu HY, Yang SY, Wei PK. Low-Cost and Rapid Fabrication of Metallic Nanostructures for Sensitive Biosensors Using Hot-Embossing and Dielectric-Heating Nanoimprint Methods. Sensors (Basel, Switzerland). 2017;17(7).
19. Lee K-L, Chang C-C, You M-L, Pan M-Y, Wei P-K. Enhancing the Surface Sensitivity of Metallic Nanostructures Using Oblique-Angle-Induced Fano Resonances. Scientific Reports. 2016;6:33126.
20. He L, Pagneux Q, Larroulet I, Serrano AY, Pesquera A, Zurutuza A, et al. Label-free femtomolar cancer biomarker detection in human serum using graphene-coated surface plasmon resonance chips. Biosensors and Bioelectronics. 2017;89:606-11.

View Article Online
DOI: 10.1039/C8AN01127C

21. Nie W, Wang Q, Yang X, Zhang H, Li Z, Gao L, et al. High sensitivity surface plasmon resonance biosensor for detection of microRNA based on gold nanoparticles-decorated molybdenum sulfide. Analytica Chimica Acta. 2017;993:55-62.
22. Schmieder S, Weißpflog J, Danz N, Klotzbach U, Sonntag F. Detection of miRNA using a surface plasmon resonance biosensor and antibody amplification. Current Directions in Biomedical Engineering2016. p. 135.
23. Mousavi MZ, Chen H-Y, Wu S-H, Peng S-W, Lee K-L, Wei P-K, et al. Magnetic nanoparticle-enhanced SPR on gold nanoslits for ultra-sensitive, label-free detection of nucleic acid biomarkers. Analyst. 2013;138(9):2740-8.
24. Mousavi MZ, Chen H-Y, Hou H-S, Chang C-Y-Y, Roffler S, Wei P-K, et al. Label-free detection of rare cell in human blood using gold nano slit surface plasmon resonance. Biosensors. 2015;5(1):98-117.
25. Lee K-L, Hsu H-Y, You M-L, Chang C-C, Pan M-Y, Shi X, et al. Highly Sensitive Aluminum-Based Biosensors using Tailorable Fano Resonances in Capped Nanostructures2017. 44104 p.
26. Ng SP, Yip YY, Wu C-ML. Biosensing with gain-assisted surface plasmon-polariton amplifier: A computational investigation. Sensors and Actuators B: Chemical. 2015;210:36-45.
27. Hanson EK, Lubenow H, Ballantyne J. Identification of forensically relevant body fluids using a panel of differentially expressed microRNAs. Analytical Biochemistry. 2009;387(2):303-14.